

Magnetic and electronic phases of $U_2Rh_3Si_5$

J. Willwater¹,¹ N. Steinki,¹ D. Menzel¹,¹ R. Reuter,¹ H. Amitsuka,² V. Sechovský³,³
M. Vališka³,³ M. Jaime^{4,*},^{4,*} F. Weickert,^{5,*},^{5,*} and S. Süllow¹

¹*Institut für Physik der Kondensierten Materie, TU Braunschweig, D-38106 Braunschweig, Germany*

²*Department of Physics, Hokkaido University, Sapporo 060-0810, Japan*

³*Faculty of Mathematics and Physics, Charles University, Ke Karlovu 5, Prague 2, Czech Republic*

⁴*National High Magnetic Field Laboratory, Los Alamos National Laboratory, Los Alamos, New Mexico 87545, USA*

⁵*National High Magnetic Field Laboratory, Florida State University, Tallahassee, Florida 32310, USA*



(Received 27 October 2020; revised 21 December 2020; accepted 21 January 2021; published 4 February 2021)

We present a detailed study of the magnetic and electronic properties of $U_2Rh_3Si_5$, a material that has been demonstrated to exhibit a first-order antiferromagnetic phase transition. From a high-magnetic-field study, together with extensive experiments in moderate fields, we establish the magnetic phase diagrams for all crystallographic directions. The possibility of an electronic phase in a narrow interval above the Néel temperature as a precursor of a magnetic phase is discussed.

DOI: [10.1103/PhysRevB.103.054408](https://doi.org/10.1103/PhysRevB.103.054408)

I. INTRODUCTION

For many years now, the variety of exotic ground states in intermetallic uranium compounds has been the focus of extensive research efforts. Special attention was given in particular to the magnetic and superconducting ground states that often are not well described by the Fermi liquid model [1–3]. Another line of research on uranium compounds involves studies on unique magnetic transitions accompanied by a structural transition, due to strong magnetoelastic interactions. Well-known examples are insulating UO_2 [4–7] and intermetallic UPd_3 [8–10].

More recently, it has been demonstrated that $U_2Rh_3Si_5$ also shows such a strong coupling between magnetic order and the lattice degrees of freedom. Various experiments suggest that it is a rare example of a $5f$ material with a first-order antiferromagnetic phase transition [11–14]. Tentatively, this was explained with the so-called bootstrapping effect, in which the crystal field splitting in combination with the magnetoelastic interactions occurring close to a magnetic transition leads to changes in the crystal field scheme [14–16]. This in turn influences the magnetic ordering and the structural behavior.

$U_2Rh_3Si_5$ crystallizes in the monoclinic $Lu_2Co_3Si_5$ structure with the space group $C2/c$ [13,17]. The monoclinic distortion is small, with a monoclinic angle of $\beta = 90.045(10)^\circ$. Therefore it is a common procedure to describe the crystal structure as a quasiorthorhombic lattice with the space group $Ibam$ (see Fig. 1). The b and c axes are perpendicular to each other, and the new direction a' is specifically chosen to be perpendicular to b and c . In the following, the direction a' will be labeled the a axis.

$U_2Rh_3Si_5$ orders antiferromagnetically at a temperature of $T_N = 25.5\text{--}25.7$ K, with the variation of T_N reflecting different references, i.e., different experimental techniques to determine this value [11–14]. Becker *et al.* observed a sharp jump in the specific heat at T_N with an amplitude of more than 100 J/(mol K) [11]. Furthermore, a neutron-diffraction study detected a sublattice magnetization jump at T_N from zero to $2/3$ of its maximum within a temperature range of 0.2 K, while x-ray diffraction measurements revealed a significant expansion of the unit cell with cooling below T_N [13]. These effects indicate a first-order magnetic transition. In addition, the magnetic structure was investigated by neutron diffraction, revealing that the magnetic moments are confined to the ab plane (see Fig. 1). More specifically, they align along the direction of the nearest-neighbor U-Rh bonds [13]. The uranium ions have a moment of $\mu = 2.35 \mu_B$, and the linear specific-heat term of $\gamma = 22$ mJ/(K² mol) suggests that they are well localized [11].

Additionally, the magnetization at 4.5 K up to 30 T was measured by Takeuchi *et al.* and shows a strong magnetic anisotropy for the different crystallographic axes [12]. Especially the magnetization for B parallel to the b axis ($B\parallel b$) is striking because of a sharp jump at 14 T. The large jumplike change in the magnetization by $1.6 \mu_B$ per U atom supports the notion of a first-order phase transition. In contrast, in these initial measurements the magnetization at 4.5 K for the configurations $B\parallel a$ and $B\parallel c$ increased linearly without any transitions up to the highest measured fields. For all axes the magnetization appeared not to be in full saturation at 30 T. For the b axis it was argued that the residual quantitative mismatch between a high-field magnetization of $1.8 \mu_B$ per U atom and an ordered magnetic moment of $2.35 \mu_B$ reflects residual moment canting in the polarized state [18]. For the other crystallographic directions the moments of a fraction of $1 \mu_B$ suggest that there must be magnetic transitions at higher fields into the fully polarized state [12].

*Present address: Physikalisch-Technische Bundesanstalt, Bundesallee 100, D-38116 Braunschweig, Germany.

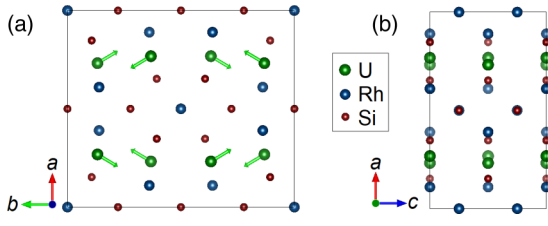


FIG. 1. Crystallographic and magnetic structure of $U_2Rh_3Si_5$ from Ref. [13] with a view of the (a) ab and (b) ac planes; for details, see text.

In this situation, here we present magnetization and axial magnetostriction measurements in pulsed magnetic fields up to 65 T to extensively characterize the magnetic phase diagrams of $U_2Rh_3Si_5$ for all crystallographic directions. For a comprehensive magnetic and electronic characterization, we include the angular-dependent susceptibility, the resistivity, the magnetoresistivity, and the thermal expansion in zero or moderate magnetic fields. With these data, we have been able to derive the magnetic phase diagrams of $U_2Rh_3Si_5$ over a large temperature and magnetic field range and have obtained new insight into the precise nature of the magnetic phase transition(s).

II. EXPERIMENTAL DETAILS

For the experiment, we used three different bar-shaped single-crystalline samples of $U_2Rh_3Si_5$ with lengths of a few millimeters and with 0.5×0.5 -mm² cross section. The samples were cut from a $U_2Rh_3Si_5$ single crystal, which was grown by a modified Czochralski method in a tri-arc furnace (see Ref. [19]) from a stoichiometric melt [U (99.9% purity), Rh (99.95% purity), Si (99.9999% purity)]. The uranium metal of 99.9% purity has been additionally purified using the solid-state electrotransport technique [20]. The pulling speed during the growth varied between 3 and 5 mm/h. The quality of the grown crystal was verified by x-ray Laue diffraction. The chemical composition of the single crystal was analyzed in a scanning electron microscope, Tescan Mira I LMH, equipped with an energy dispersive x-ray (EDX) detector, Bruker AXS, inspecting the signal both of the secondary and backscattered electrons. Elemental mapping by EDX confirmed good composition homogeneity of the as-grown crystal. The average of multiple point scans from different parts of the sample provided the U:Rh:Si composition of 2.2(5):3.0(2):4.8(5).

The axial magnetostriction and magnetization were measured in pulsed magnetic fields up to 65 T in a temperature range from 1.4 to 30 K at National High Magnetic Field Laboratory (NHMFL) at Los Alamos National Laboratory. An optical fiber with Bragg gratings was used for the measurement of the axial magnetostriction as a function of the magnetic field and the thermal expansion in zero field as a function of the temperature as described in Refs. [21–23]. The relative values of the magnetization were measured up to 65 T using a pickup coil technique [24]. Subsequently, the magnetization was scaled onto measurements taken in a commercial SQUID magnetometer up to 5 T. In addition, the

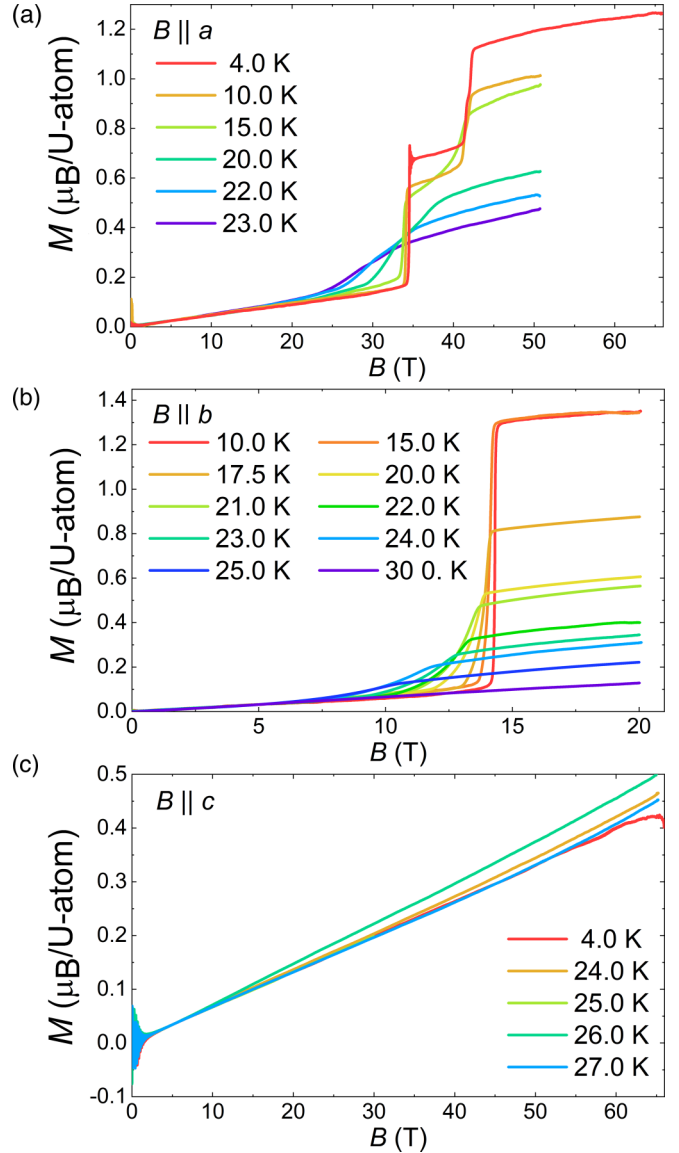


FIG. 2. Magnetization of $U_2Rh_3Si_5$ in pulsed magnetic fields for (a) $B \parallel a$, (b) $B \parallel b$, and (c) $B \parallel c$ at different temperatures; for details, see text.

angular-dependent susceptibility has also been measured in a SQUID magnetometer with a field of 0.1 T.

Moreover, ac resistivity measurements in four-point configuration were carried out to determine the magnetoresistivity and the temperature dependence of the resistivity in magnetic fields up to 9 T for all crystallographic axes.

III. RESULTS

A. High-field measurements

The magnetization of $U_2Rh_3Si_5$ for the different crystal axes up to 65 T is shown in Fig. 2. Overall, there is significant anisotropy to be seen in the data. Absolute values at highest fields vary between $0.5 \mu_B$ (c axis) and $1.4 \mu_B$ per U atom (b axis). The latter value is reasonably close to the one reported by Takeuchi *et al.* [12] for the same field direction. Furthermore, while field-induced transitions are observed for $B \parallel a$ and

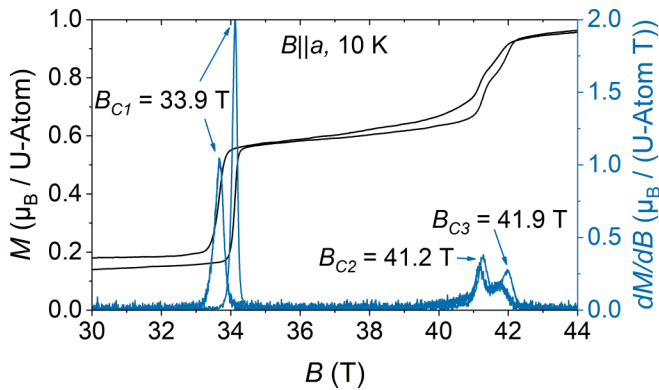


FIG. 3. High-field range of the magnetization and dM/dB for $B||a$ at 10 K. The critical fields were obtained by averaging over the values of the field up-sweep and field down-sweep; for details, see text.

$B||b$, this is not the case along the c axis. The different features will now be discussed in detail.

For the field $B||a$ we observe two jumps in the magnetization. At lowest temperatures, after a small linear increase the first jump appears at 34 T from $0.1 \mu_B$ up to a value of 0.6 – $0.7 \mu_B$ per U atom, and the second occurs at approximately 42 T with roughly the same increase of the magnetization. Closer inspection of the upper transition reveals that it appears as a two-step process by itself with two transition fields about 1 T apart (see Fig. 3). It might be argued that this two-step feature is extrinsic, arising, for instance, from a twinned crystal with two slightly different critical fields. In that case, however, the lower transition at B_{C1} should also be split into two, which is not the case; this suggests the feature to be intrinsic.

Above the upper transitions, for higher fields the magnetization increases again linearly with the field and is of a magnitude similar to that of the b -axis magnetization. Following the argument of Galli *et al.* [18], this would imply that also for the a axis in high fields the magnetic moments are still canted with respect to the external field. The value of the maximal magnetization decreases as temperature is increasing, and the jumps broaden significantly. Again, the sharp magnetization jumps indicate first-order transitions. The transition fields used to construct the magnetic phase diagram (see below) were determined by averaging the critical field values of the field up-sweep and field down-sweep. These were obtained from local maxima in dM/dB (see Fig. 3).

For the configuration $B||b$ and lowest temperatures, only one jump by $1.3 \mu_B$ per U atom at a field of 14 T is observed. In high fields, the maximal magnetization hardly changes for increasing temperature up to 15 K but then decreases strongly. Additionally, the transition shifts to lower fields and broadens significantly. Again, there is an intrinsic hysteresis between the field up-sweep and field down-sweep. The transition field is also determined as maximum in dM/dB .

In the measurement of the magnetization for $B||c$ there is no phase transition visible. The magnetization increases almost linearly with the magnetic field up to $0.5 \mu_B$ per U atom at 65 T at the lowest temperatures, and there are hardly differences for measurements at different temperatures. Moreover, it appears as if the magnetization has a small upwards

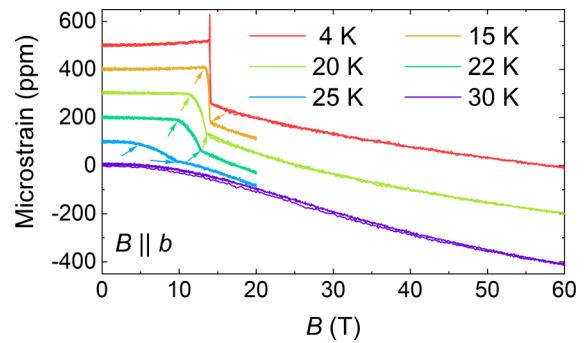


FIG. 4. Axial magnetostriction of $U_2Rh_3Si_5$ for magnetic fields along the b axis for different temperatures up to 60 T (for clarity, data are shifted with respect to each other by 100 ppm); for details, see text.

curvature. It might be considered a precursor behavior for a magnetic transition to occur at even higher fields.

For additional information about the interdependence between the structure and the magnetic behavior, we investigated the axial magnetostriction for $B||b$ in fields up to 60 T. The corresponding measurements along the other crystallographic axes failed because of the strong magnetic anisotropy of the samples. For field directions away from the easy magnetic axis, it leads to magnetic torque on the sample, significantly twisting it on the fiber used for the magnetostriction experiment and thus affecting the experiment.

The measurements of the magnetostriction in terms of Microstrain $\Delta l/l$ (with $\Delta l =$ change of length l of the sample) for $B||b$ at different temperatures is shown in Fig. 4 (for clarity, data are shifted with respect to each other by 100 ppm). At low temperatures (4 K) the transition observed in the magnetization is clearly identified by a drop in the microstrain by 250 ppm at 14 T. As the temperature is raised, the magnitude of the drop decreases, and the transition becomes wider and seems to transform into a two-step transition. The arrows in Fig. 4 were determined as the points, where a local extremum is detectable in the second field derivative of the microstrain. This broadening of the transition is also visible in the magnetization (as shown in Fig. 5), where with rising temperatures the transition changes from the low-temperature steplike behavior

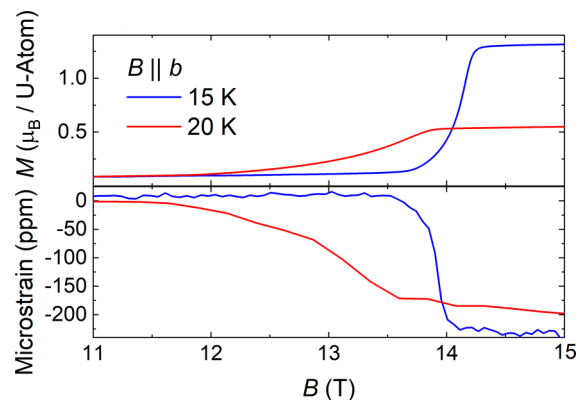


FIG. 5. Comparison of the magnetization and the magnetostriction at 15 and 20 K for $B||b$; for details, see text.

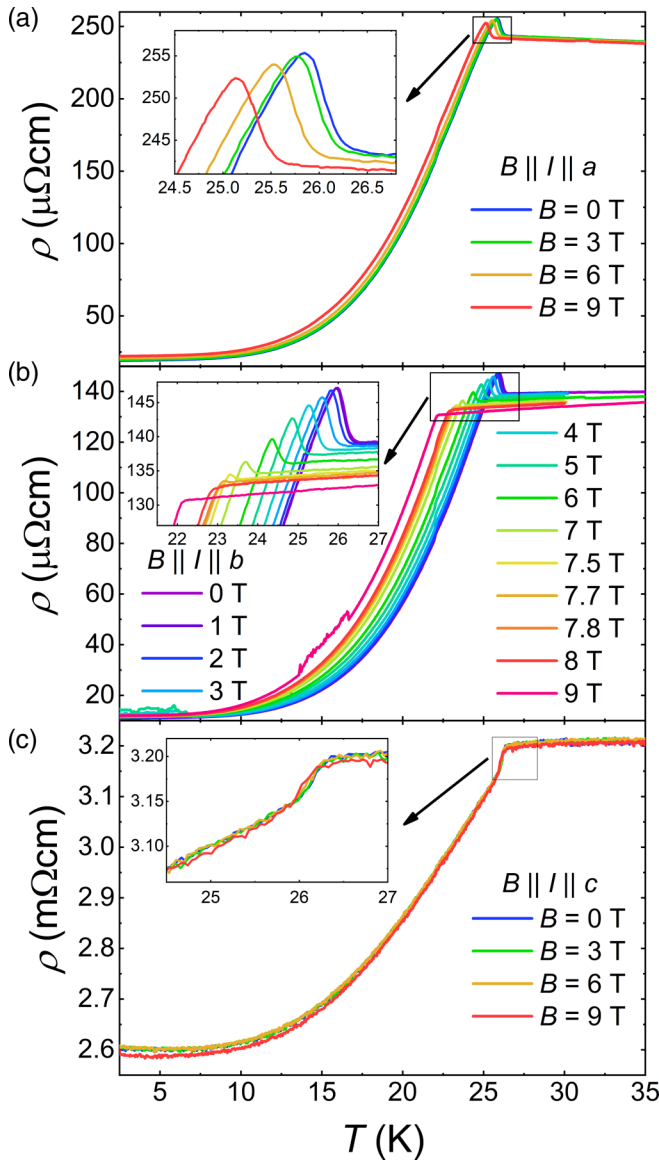


FIG. 6. Resistivity of $\text{U}_2\text{Rh}_3\text{Si}_5$ as a function of temperature for the (a) a , (b) b , and (c) c axes in different magnetic fields up to 9 T; for details, see text.

into a more S-shaped form. The field value of the “high-field side” of the magnetostrictive transition is in very good agreement with the turning point in the magnetization along the b axis, while the feature at the “low-field side” of the magnetostrictive transition appears to match the beginning of the upturn in the magnetization. Because the transitions in the magnetization along the a axis exhibit a similar broadening with temperature, we suspect that the behavior of the magnetostriction for $B||a$ is similar to that for $B||b$.

B. Resistivity

To link our high-field data on the magnetic phase diagram with the low-field behavior of $\text{U}_2\text{Rh}_3\text{Si}_5$, as a next step we measured the resistivity as a function of the temperature for different magnetic fields along the three axes (Fig. 6). The residual resistivity ρ_0 values of approximately $20 \mu\Omega \text{ cm}$ for

the a axis and $10 \mu\Omega \text{ cm}$ for the b axis are similar to those reported in Ref. [11] and indicate good sample quality. In contrast, the sample along the c axis shows a much higher residual resistivity of $2.6 \text{ m}\Omega \text{ cm}$. Previously, much smaller values have been reported for this axis [11]. As our c -axis crystal stems from the same batch as the other two samples, we believe that this particular sample is microcracked, possibly as result of being cycled multiple times through the first-order phase transition during the measurements, in this way likely affecting the absolute value of the resistivity for this crystallographic direction. This is supported by the fact that the residual resistivity ρ_0 for the c axis was lower in a first measurement.

There are various peculiarities in the resistivity visible. In the measurements along the a and b axes an anomaly around the transition temperature is noticeable. In detail [see insets of Figs. 6(a) and 6(b)], in zero field the resistivity increases with decreasing temperature below $T^* = 26.4 \text{ K}$ for the a -axis measurement and $T^* = 26.5 \text{ K}$ for the b -axis measurement, i.e., slightly above the antiferromagnetic (AFM) transition temperature. Here, the critical temperature T^* of the upturn was determined as the maximum in the second temperature derivative of the resistivity. Only after cooling by 0.5 K , i.e., down to T_N , the resistivity turns over and decreases steeply. The maximum is found at a temperature of 25.9 K for the a -axis measurement and 26.0 K for the b -axis measurement.

In an external magnetic field along the a axis the anomaly slightly shifts to lower temperatures [see inset of Fig. 6(a)]. For the configuration $B||b$ the anomaly changes much more rapidly with increasing magnetic field [inset of Fig. 6(b)]. First, a shift to lower temperatures with magnetic field is visible. In addition, the width and the height of the peaklike anomaly decrease with increasing field. At a field of 7.8 T the anomaly is not visible any more, and the resistivity immediately decreases at the transition temperature. In contrast, there is no peaklike anomaly measured for the c axis. The resistivity instead exhibits a relatively sharp downturn at the temperature where the upturn in the resistivity is visible for the a and b axes, and it shows a kink at T_N . External magnetic fields up to 9 T along the c axis have no impact on these features.

Previously, Becker and co-workers [11,25] measured the resistivity in zero field for the three axes and in fields up to 20 T for the b axis. In their interpretation, the peaklike anomaly was associated with the opening of a superzone gap due to antiferromagnetic ordering, as is observed in erbium and terbium [26]. Such a gap leads to a rounded maximum of the resistivity just below the transition temperature as the result of a modified Brillouin zone in the magnetically ordered phase. The drop in the resistivity upon further lowering the temperature then is due to the reduction of phonon and magnon scattering. This interpretation seems to match the fact that the anomaly is only visible for the a and b axes. The magnetic moments lie in the ab plane, and therefore the unit cell only doubles along the a and b directions at the antiferromagnetic transition.

However, there are significant differences to superzone gap occurrences such as for erbium and terbium [26]. In $\text{U}_2\text{Rh}_3\text{Si}_5$, the upturn in the resistivity for the a and b axes and the downward drop for the c axis take place at a temperature of 0.5 K above the transition temperature T_N . Moreover, at

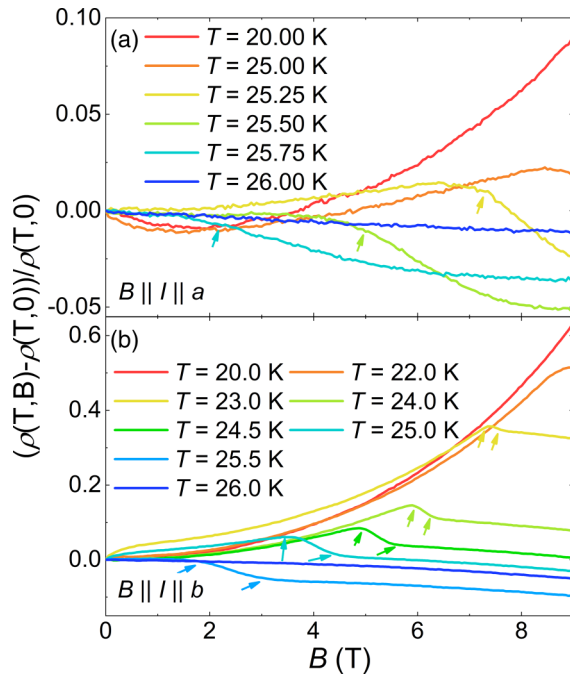


FIG. 7. Longitudinal magnetoresistivity of $\text{U}_2\text{Rh}_3\text{Si}_5$ for magnetic fields along the (a) a axis and (b) b axis for different temperatures up to 9 T; for details, see text.

T_N , the resistivity of our U compound for the a and b axes shows a kinklike downturn, while for the c axis we observe a change in slope. This is in contrast to the rounded maxima seen in erbium and terbium and predicted by theory [27]. In addition, an external magnetic field does not lead to a gradual disappearance of the gap (see other materials with a superzone gap such as terbium [28] or URu_2Si_2 [29]). After all, the resistive feature associated with the occurrence of a superzone gap is related to the change in the translationally invariant cell in the antiferromagnetic phase, which is not a continuous function of the magnetic field. In conclusion, the interpretation of the peaklike anomaly in $\text{U}_2\text{Rh}_3\text{Si}_5$ as being the result of a superzone gap may be incorrect, and other effects appear to be responsible for the peculiar behavior of the resistivity around the transition temperature. We note that while the discrepancy between the upturn temperature T^* and the antiferromagnetic transition temperature T_N in $\text{U}_2\text{Rh}_3\text{Si}_5$ was not reported before, close inspection of the plots in Ref. [11] suggests that a similar discrepancy exists for those data.

Finally, the longitudinal magnetoresistivity (MR) along the three crystallographic axes was measured. In Fig. 7 we plot the normalized magnetoresistivity as a function of the external magnetic field for different temperatures. We omit the magnetoresistivity measured for $B \parallel c$, as there was no resolvable signal beyond experimental scatter, this likely being the result of the large extrinsic residual resistivity for this axis.

The magnetoresistivity is highly anisotropic. For instance, at 20 K we find a MR {defined as $[\rho(T, B) - \rho(T, 0)]/\rho(T, 0)$ } of up to about 10% along the a axis, while along b it reaches 60%. This obviously reflects the much stronger field dependence of T_N along the b axis

than along a and is consistent with the temperature-dependent resistivity measurements (Fig. 6), where a magnetic field caused large changes in the resistivity for the b axis and only moderate changes for the a axis.

Still, the measurements for the configurations $B \parallel a$ and $B \parallel b$ show a qualitatively similar behavior. In detail, discussing the b -axis data, starting from high fields and for temperatures in the range from 23 to 26 K, the magnetoresistivity rises monotonously upon lowering the field down to the upper critical field. At the critical field there is a two-step transition visible (indicated by arrows in Fig. 7). First the slope of the magnetoresistivity changes and rises more steeply until a local maximum develops. This two-step transition corresponds to the feature in the temperature-dependent resistivity (Fig. 6). The upturn in the resistivity shows up as a change in the slope of the magnetoresistivity, and the maximum in the resistivity is visible as a maximum in the magnetoresistivity. After this maximum the magnetoresistivity falls off monotonously. For the a -axis data, only the local maximum in the MR is clearly visible, while the change in slope is not easily identified. This, however, might simply reflect the stretched field scale for the a axis compared with b , making it harder to identify the upper critical field in the experimental window we access.

C. Susceptibility

Since the magnetization and magnetostriction experiments revealed a very large magnetic anisotropy, we measured the angular-dependent susceptibility in small magnetic fields (0.1 T). Figure 8 shows the susceptibility of $\text{U}_2\text{Rh}_3\text{Si}_5$ in emu per mole of uranium (mol U) as it is rotated from the b axis in 10° steps towards the a and the c axes, and for the corresponding rotation from the c towards the a axis.

For high temperatures the susceptibility shows a Curie-like behavior down to $T_N = 25.8$ K, where the susceptibility drops because of the antiferromagnetic transition. The almost step-like behavior at the transition supports the assumption of a first-order transition. As noted before, the anisotropy between the three axes is very large. In the paramagnetic phase the biggest susceptibility response is detectable for the b axis with a maximum of the susceptibility at T_N of 0.035 emu/mol U, while for the a (c) axis the maximum susceptibility is a factor of 3 (7) smaller. Therefore we conclude that the b axis is the magnetically easiest and the c axis is the hard axis. The anisotropy in the magnetically ordered phase is consistent with this view and the reported magnetic structure, as the magnetic moments are oriented within the ab plane with an angle of 34° to the b axis.

To complete our investigation of the phase transitions, we measured the temperature-dependent susceptibility in fields up to 5 T and compare it with the corresponding resistivity data in Fig. 9. Beginning with the a axis, the susceptibility transition shifts only moderately to lower temperatures from $T_N = 25.8$ K at 0.1 T to $T_N = 25.6$ K at 5 T. The transition temperature was determined as the onset of the change in slope of the susceptibility upon lowering temperatures from above T_N . The absolute values of the susceptibility differ only slightly for the measurements in different fields, with a tendency to an increase in the height of the steplike transition

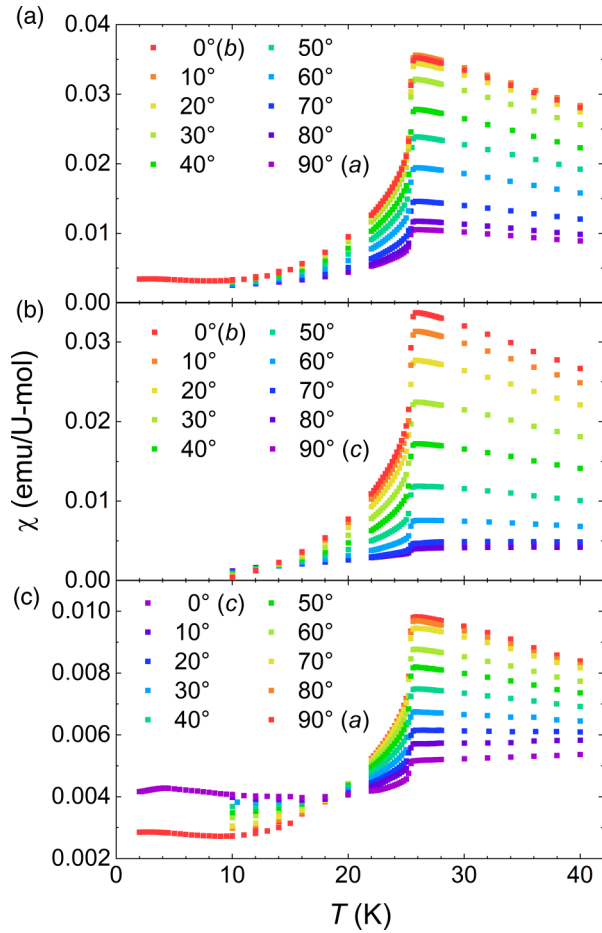


FIG. 8. Angular-dependent measurements of the susceptibility with 10° steps for rotations from (a) the b to the a axis, (b) the b to the c axis, and (c) the c to the a axis; for details, see text.

at T_N . An exception is the measurement at 0.1 T, which is about 0.5 memu/mol U larger than those at higher fields. This might reflect a residual contribution from a small number of paramagnetic impurities, which are saturated in higher fields.

In comparison, the influence of the magnetic field on the b -axis susceptibility is stronger. While $\chi(T)$ decreases approximately by 0.014 emu/mol U in 0.1 T at the transition from paramagnetism into the antiferromagnetic phase, it decreases by 0.018 emu/mol U in 5 T with a transition temperature of $T_N = 24.5$ K. Thus the AFM transition in the susceptibility shifts to lower temperatures and is more pronounced for higher fields. Finally, the susceptibility for the c axis shows basically no field dependence up to 5 T. Only, similar to the a axis, the susceptibility at 0.1 T is a bit higher possibly because of paramagnetic impurities.

To illustrate the field dependence of the antiferromagnetic transition seen in the susceptibility and resistivity, in Fig. 9 we include the latter quantity. The comparison shows that the transition temperatures in the susceptibility for the a and b axes are in reasonably good agreement [30] (difference of 0.1–0.2 K) with the maxima in the resistivity measurements, and not with the upturn in ρ . Therefore it supports our conclusion that the upturn in the resistivity is not due to the antiferromagnetic transition. Analogously, the transition temperature of the c axis in the susceptibility fits better the

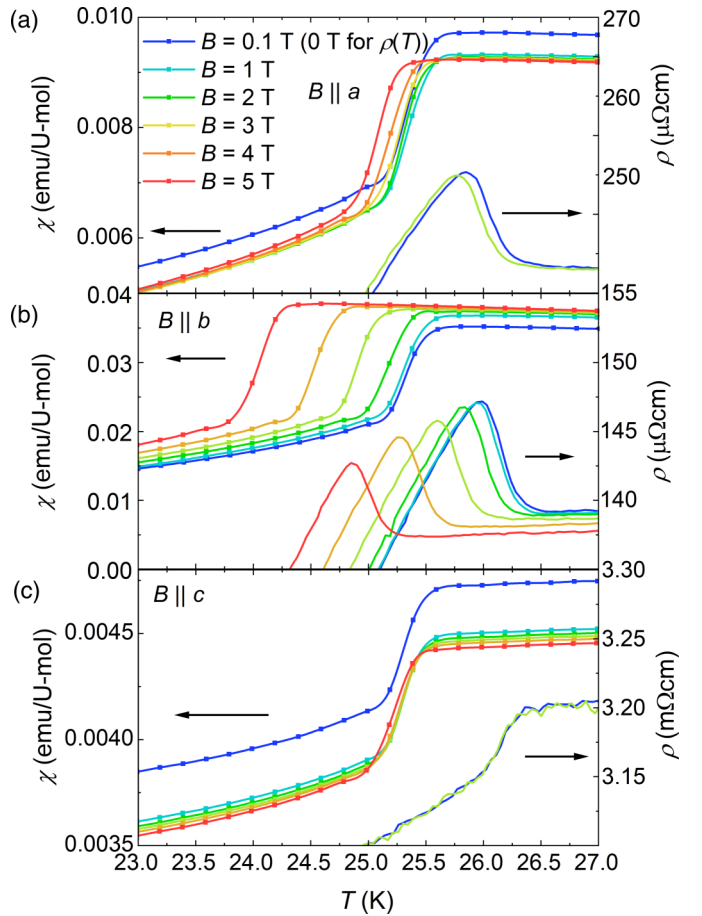


FIG. 9. Measurements of the susceptibility for (a) $B \parallel a$, (b) $B \parallel b$, and (c) $B \parallel c$ between 23 and 27 K for fields up to 5 T. For direct comparison the corresponding resistivity measurements already shown in Fig. 6 are included; for details, see text.

second change in the slope of the resistivity, when coming from higher temperatures.

D. Thermal expansion

In order to affirm the results from previous x-ray diffraction experiments [13], we measured the thermal expansion in zero magnetic field. In Fig. 10 we present the thermal expansion $\Delta l/l$ in ppm as a function of temperature from 20 to 30 K for the three axes. With cooling down, the unit cell of $U_2Rh_3Si_5$ expands slightly in the a and c directions and contracts along the b axis. At the antiferromagnetic transition temperature of 25.8 K the thermal expansion changes drastically along all axes, leading to an expansion along the b and c axes and a contraction along the a axis. The change in the thermal expansion is approximately $\delta_a = 38$ ppm, $\delta_b = -29$ ppm, and $\delta_c = -39$ ppm within 0.8 K of T_N . After this jump in $\Delta l/l$ the unit cell further expands along the c axis and contracts along the a and b axes.

Our thermal expansion measurement is in very good agreement with the measurement of the lattice parameters by x-ray diffraction [13]. The pronounced jump in the thermal expansion is triggered by the antiferromagnetic first-order transition. Notably, the transition temperature is similar to

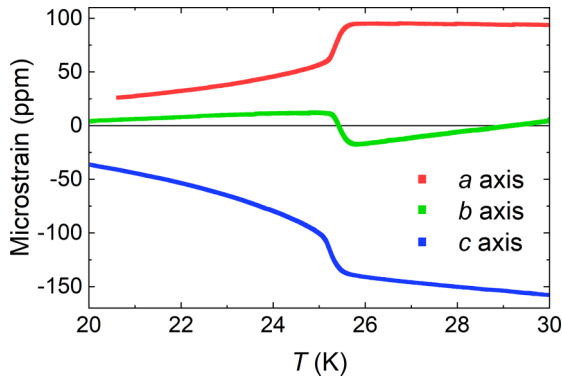


FIG. 10. Thermal expansion of $U_2Rh_3Si_5$ in zero field along the three crystallographic axes; for details, see text.

the susceptibility at 25.8 K [30]. Thus the lattice response in $U_2Rh_3Si_5$ is directly impacted by the magnetism. This supports our assumption that the maximum in the resistivity at 25.8 K is due to the magnetic first-order transition and the upturn in the resistivity for the a (b) axis at 26.4 (26.5) K is caused by something different.

E. Magnetic phase diagram

From our data we construct the magnetic phase diagram of $U_2Rh_3Si_5$ for magnetic fields up to 65 T in Fig. 11. The data points have been collected from magneti-

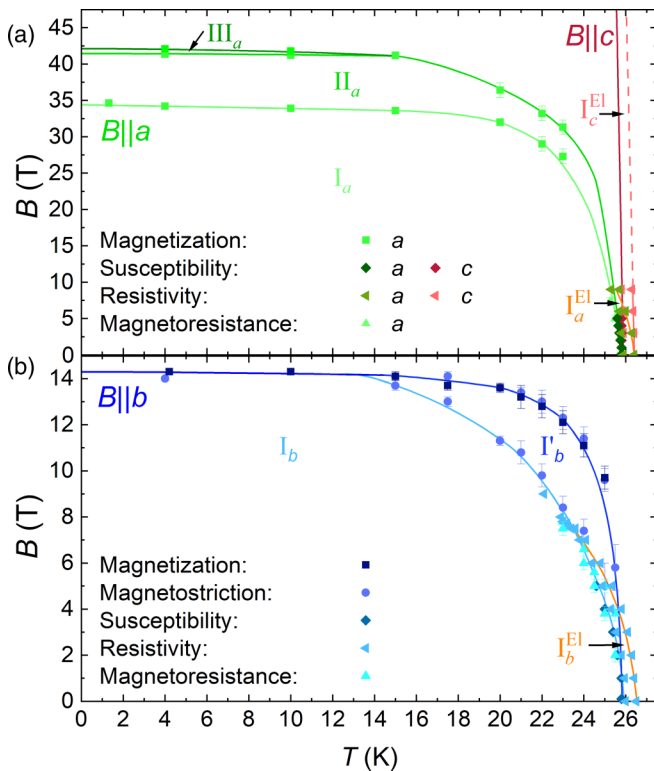


FIG. 11. Phase diagram of $U_2Rh_3Si_5$ for (a) the a and c axes and (b) the b axis over a wide temperature and magnetic field range. The solid lines are guides to the eye denoting phase borderlines, while the dashed lines are suspected phase borderlines; for details, see text.

zation, magnetostriction, magnetic susceptibility, resistivity, and magnetoresistivity data as described above. We start by discussing the magnetically ordered phases.

In zero field, AFM order sets in below $T_N = 25.8$ K. The AFM ground-state phase is labeled I_a along the a axis and, correspondingly, I_b along the b axis [Fig. 11(a)]. Notably, in magnetic fields there is a clear and pronounced anisotropy visible for the different axes. The phase boundary for the AFM phase I_a at low temperatures is found at 34 T, while the phase boundary for I_b lies only at fields of 14 T. In contrast, there was no phase transition observed for the c axis up to 65 T in the magnetization, implying that for this axis below T_N and the experimental field range the system is always in AFM phase I.

For the c -axis data, we note that no phase boundary has been crossed even at 25 K in 65 T. If we compare this observation with the a - or b -axis data, where at 25 K the critical field is of the order of half of the zero-temperature value, it implies that for the c axis the corresponding zero-temperature critical field value would be about 100 T or more. Thus, overall, we find an anisotropy of the critical fields of $U_2Rh_3Si_5$ of at least a factor of 5 between the b and c axes.

We will now discuss the details of these phase diagrams, starting with the magnetic transitions of the a axis. There are two clear jumps visible in the magnetization measurement (with the upper one of these jumps being a two-step transition at low temperatures), and therefore we assume that these are first-order transitions. The new phase II_a [Fig. 11(a)] was measured for a broad temperature and magnetic field range. The borderlines of phases I_a and II_a basically evolve parallel to each other with a distance of 7–8 T up to a temperature of about 15 K. Then, for temperatures up to $T_N = 25.8$ K, the critical fields rapidly drop to zero. Additionally, the two-step transition measured in the magnetization at 4 and 10 K reflects a narrow phase III_a with a width of 1 T prior to the field-polarized phase. Since the two-step transition is not visible in the magnetization at 15 K, we assume that phase III_a only exists up to a temperature of 10–15 K.

In comparison, for the easy axis, i.e., the b axis [see Fig. 11(b)], we resolve additional peculiarities. Our measurements reveal a first-order phase transition at 14 T for low temperatures. At the phase transition the magnetic moments flip from AFM phase I_b into a field-polarized phase. Surprisingly, in the magnetostriction the steplike drop observed at the lowest temperatures transforms into a double transition (Fig. 4) in the temperature range from 15 to 25.8 K, denoting a distinct phase range I'_b [Fig. 11(b)]. This change in the field-dependent behavior is also reflected in the magnetization, which in this temperature range exhibits the more gradual character of a metamagnetic transition, which starts at the borderline $I_b \rightarrow I'_b$. At the upper boundary of phase range I'_b , visible in the magnetization as magnetic saturation and in the magnetostriction as a gradually flattening behavior, the magnetic moments flip into the field-polarized state.

The magnetization of the a axis shows a similar gradual character of the metamagnetic transition in a similar temperature range. Therefore we assume that the a axis exhibits a phase range I'_a equivalent to I'_b for the b axis. As we will discuss below, in particular, resistivity measurements in fields up to ~ 25 T should be a suitable tool to identify this phase range.

Finally, we address the c -axis data, where we have only been able to find a transition in the temperature-dependent susceptibility and resistivity, but not in the field-dependent magnetization. From our nonobservation of a phase transition in our pulsed-field experiments we conclude that the magnetic fields have not been strong enough to align the magnetic moments along the c axis. This thought is supported by the alignment of the magnetic moments in the ab plane in zero field reported in Ref. [13]. Therefore the phase boundary for the c axis is very steep as indicated by the red line in Fig. 11(a).

Aside from the transitions detected in thermodynamic or structural properties, in addition, very unusual features are visible in the resistivity. As pointed out, the upturn in the resistivity with decreasing temperature for the a and b axes and the downward jump for the c axis are at slightly higher temperatures T^* than T_N . Moreover, these anomalies appear not to be visible in the susceptibility, thermal expansion, and magnetization measurements. We plot the field evolution of this transition with an orange (red) line for the a (c) axis in Fig. 11(a) and with an orange line for the b axis in Fig. 11(b). A close look at the b axis indicates that for zero or low magnetic fields this phase borderline is clearly distinct from both the phase boundaries I_b - I'_b and I'_b -paramagnetic phase (PM). However, with increasing field this transition merges into the lower phase borderline I_b - I'_b . The merger denotes the point where no upturn in the temperature-dependent resistivity is seen any more, i.e., at 7.8 T. Thus, from our data, we conclude that for the b -axis experiment there is even a distinct third phase in the phase diagram of $U_2Rh_3Si_5$, i.e., phase I_b^{El} . As it is only detected in the resistivity, it appears to be an electronic rather than a magnetic transition.

Given that along the a axis the overall resistive behavior is very similar to that along the b axis, it is likely that also for this axis in higher fields the upturn in the resistivity disappears. The behavior would then be analogous to the b axis, implying that also for this crystallographic direction there appears a distinct phase I_a^{El} [see Fig. 11(a)]. Here, additional resistivity measurements in higher fields up to the 20-T range are called for. Finally, while for the c axis the experimental data are less abundant, the temperature range of the almost steplike reduction of the resistivity similarly would signal a distinct electronic phase I_c^{El} [Fig. 11(a)] for this crystallographic direction.

IV. DISCUSSION

We will now summarize our experimental findings and discuss the implications of the new observations. Overall, from the broad characterization of our single-crystalline samples $U_2Rh_3Si_5$, their physical properties correspond to those previously reported. In particular, our measurements fully agree with the notion of a first-order nature of the antiferromagnetic transition at T_N [11–14].

Notably, we observe a new feature in the resistivity that seems to require an explanation in terms of an electronic phase of unknown origin in $U_2Rh_3Si_5$ and that appears as a precursor phase of the magnetic transitions. After all, there seems to be a very close interdependence of electronic, magnetic, and structural degrees of freedom in $U_2Rh_3Si_5$, which will require

additional studies to fully understand. However, prior to a more detailed discussion of the unusual electronic behavior seen in the present set of experiments, we will first summarize and evaluate the apparently more common findings on the magnetic (and structural) properties.

Starting with the observations on the phase diagram of $U_2Rh_3Si_5$, for the first time, various steps in the high-field magnetization of the a axis were observed, establishing the existence of a rather complex magnetic phase diagram for this crystallographic direction. In detail, we conclude that the ground-state AFM phase I_a transforms with a first-order transition into phase II_a . At higher fields, again there is first-order character at the transition from phase II_a into the paramagnetic phase. As a subtlety, this transition even has double-step character, implying that there is a very narrow intermediate magnetic phase III_a . Correspondingly, phases II_a and III_a must be intermediate between the AFM alignment of phase I_a and the polarized spin state of the paramagnetic high-field phase. Likely, there is additional staggering of magnetic moments in these field-induced phases compared with the AFM phase I_a , for instance, with a stacking of moments such as up-up-down, etc., as discussed, for instance, for the staircase magnetization scenario in CeSb [31].

For the b axis at low temperatures the high-field magnetization and magnetostriction show a single magnetic transition connected with a large volume change. This appears qualitatively to be consistent with the bootstrapping scenario [11–14]. However, on top of this, the phase diagram for the b axis exhibits various particularities. At temperatures ≤ 10 K and high fields the transition from phase I_b in the paramagnetic phase has a clear first-order character demonstrated by sharp jumps in the magnetization and magnetostriction. However, for higher temperatures in these measurements the transition becomes broader and transforms into a two-step transition, in this way defining an intermediate phase range I'_b . From their appearances, in this temperature and field range the magnetic transitions $I_b \rightarrow I'_b$ and $I'_b \rightarrow$ PM have more of a second-order or mixed-phase character, while in fields $B \rightarrow 0$ T and temperatures close to T_N the steplike temperature dependence of the susceptibility again signals a first-order transition. Finally, for the c axis, no field-induced transitions have been recorded up to 65 T, attesting to the very large magnetic anisotropy of this material.

Over the years, a number of U intermetallics, namely, UNiAl [32], UPt₂Si₂ [33,34], UN [35], USb₂ [36], UIrSi₃ [37], and UIrGe [38], have emerged with a similar change from a second-order-like to a first-order magnetic transition at low temperatures and high fields. This leads to tricritical points in the magnetic phase diagrams for these materials [34–38]. In the following we will briefly compare the reports for these materials with $U_2Rh_3Si_5$.

The mentioned materials all have an AFM ground state with Néel temperatures between 16.5 K (UIrGe) and 202 K (USb₂) [32–39]. Starting with the field-dependent magnetization, they have in common a sharp jump at the corresponding critical fields for low temperatures, indicative of a first-order phase transition [32,33,35–38]. With higher temperatures the transitions shift to lower fields and transform into an S-like shape indicating a more gradual transition into the polarized states [33,35–38]. This is similar to our measurements

on $U_2Rh_3Si_5$ as shown in Fig. 2. However, there are also differences visible, i.e., in the low-field susceptibility. While $U_2Rh_3Si_5$ shows a sharp jump at the critical temperature (see Fig. 8), the other materials exhibit a smooth rise of the susceptibility up to the critical temperature typical for the second-order phase transition in common antiferromagnets [32,33,37,38,40,41]. Only for UIrGe, in Ref. [38], do the temperature-dependent susceptibility values, measured in different magnetic fields, display a sharp upturn for higher fields. This was interpreted as a change of the transition from second to first order. The susceptibility of $U_2Rh_3Si_5$ resembles the high-field behavior of UIrGe, reflecting that at T_N , $U_2Rh_3Si_5$ exhibits a first-order transition. In summary, regarding the magnetic properties, there are various U systems with tricritical points in the magnetic phase diagram showing similarities to $U_2Rh_3Si_5$. Especially, the change of the transition in the magnetization to low temperatures indicates that $U_2Rh_3Si_5$ may exhibit tricritical points in the phase diagram for the a and b axes.

Regarding the interpretation of the first-order antiferromagnetic transition in $U_2Rh_3Si_5$ being the result of a bootstrapping effect [11,15,16], the question arises as to whether based on our experiments we can draw conclusions as to the validity of the argument. Globally, our experimental findings appear to be consistent with a bootstrapping scenario: The magnetic properties of $U_2Rh_3Si_5$ would classify this material as a uranium intermetallic with well-localized f electrons. In principle, a description of the f states within a conventional crystal electric field scheme appears possible and has been proposed before [14]. Hence it should also be possible to extend the modeling to include the field-dependent effects that we report here. Unfortunately, the low crystallographic symmetry and complex magnetic structure, together with the very pronounced local anisotropy of the f electrons, complicate matters to the effect that a detailed and quantitatively accurate modeling of the various thermodynamic properties still appears not attainable. Thus, while being consistent with the bootstrapping scenario, at present our experimental data do not yield definite proof of it.

Aside from the magnetic transitions, the upturn in the resistivity of $U_2Rh_3Si_5$ for $B\parallel a$ and $B\parallel b$ and corresponding drop along the c axis at a temperature $T^* > T_N$ denote yet another phase transition. It is observed in the resistivity but does not show a signature in the susceptibility or the structural parameters. Therefore it is not a magnetic transition, i.e., an ordering transition in spin space. Instead, the anomalies in the resistivity signal an electronic phase transition, resulting in a change in the carrier density or the scattering cross section due to band structure modifications. We note that for such electronic transitions it is a common occurrence for a phase transition to be clearly observable only in experimental probes such as electronic transport, but not in thermodynamic quantities.

Compared with $U_2Rh_3Si_5$, the resistivities of UNiAl [32], UN [40], and UIrGe [39] show some interesting similarities close to T_N . The resistivity of the c axis of UNiAl exhibits a peaklike anomaly comparable to the feature in $U_2Rh_3Si_5$. Unfortunately, from the data shown in Ref. [32] it cannot be assessed whether the magnetic transition corresponds to the upturn or the maximum of the resistivity. For a better comparison with $U_2Rh_3Si_5$ a more accurate and

field-dependent measurement of the resistivity is necessary. In UN and UIrGe, similar structures in the resistivity are visible [39,40]. For these materials, it is established experimentally that the rise of the resistivity is connected to the AFM transition temperature, and not the maximum. Here, too, it would be interesting to investigate in more detail the interplay of the electronic and magnetic behavior and compare it with $U_2Rh_3Si_5$. Altogether, based on our results on $U_2Rh_3Si_5$, it seems worthwhile to reinvestigate UNiAl, UN, and UIrGe, to verify that the features in the resistivity truly correspond to an AFM transition.

Conversely, we note that the electronic phase seen in zero magnetic field at $T^* > T_N$ sets $U_2Rh_3Si_5$ apart from all other materials. Qualitatively, the zero-field resistive behavior at T^* does have a resemblance to a charge density wave as seen, for example, in $Lu_5Ir_4Si_{10}$ [42,43]. Only, in $U_2Rh_3Si_5$, there is a very strong field dependence of the transition temperature T^* : It evolves in a fashion similar to antiferromagnetic transitions, as it shifts to lower temperatures with magnetic field. For a charge density wave, one would not expect such a field dependence, implying that an explanation of the observations along these lines appears impossible. Hence the anomaly at T^* denotes an electronic state in $U_2Rh_3Si_5$ of as yet unknown type.

Remarkably, the field dependence of the phase borderline of T^* is even somewhat stronger than that of the AFM phases. This results in a coexistence regime of electronic and magnetically ordered phases. Specifically, we have observed that the novel electronic phase transition in $U_2Rh_3Si_5$ merges with the magnetic phase transitions. This finding raises questions about our above statement of well-localized f electrons in this compound. At around the merger of the phase borderlines of T^* and I_b/I_b' , the overall behavior of the corresponding physical properties appears to be more in line with a second-order phase transition. Notably, in this range the magnetization transition smears out and does not have such a pronounced local-moment character as it has at low temperatures. It appears as if the coexistence of local-moment magnetism with an (itinerant?) electronic phase weakens the local-magnetic-moment character. Conversely, the observed strong field dependence of the transition temperature of the electronic phase would then still attest to the residual local-moment character of the U ions.

This observation of course directly relates to the issue of the proper description of uranium f magnetic moments, which can have localized, itinerant, or even dual character. A bootstrapping scenario in the presence of a dual character of the f electrons would necessarily lead to a complex interplay of local-moment physics and band structure effects. We speculate that the subtle balance of electronic and magnetic phases observed in $U_2Rh_3Si_5$ may reflect such a scenario. In this situation, experimentally what is required as a next step (and is notoriously hard to attain in uranium compounds) would be experimental information about the local-moment character of the uranium f electrons and the band structure. Additionally, the possible electric transition should be investigated by further electrical measurements such as measurements of the Seebeck effect, Hall effect, or thermal conductivity. Moreover, experiments at higher fields for the a axis, for instance resistivity measurements, might provide additional insight into this complex topic.

ACKNOWLEDGMENTS

The crystal was grown and characterized in the Materials Growth and Measurement Laboratory (MGML), which is supported within the Czech Research Infrastructures program (Project No. LM2018096). A portion of this work was performed at the Pulsed Field Facility of the National

High Magnetic Field Laboratory, which is supported by National Science Foundation Cooperative Agreement No. DMR-1157490 and DMR-1644779, the State of Florida, and the US DOE. M.J. acknowledges support by the US Department of Energy Science of 100 tesla BES program. S.S. acknowledges support by the Magnet Lab Visiting Scientist Program of the NHMFL.

- [1] C. Pfleiderer, *Rev. Mod. Phys.* **81**, 1551 (2009).
- [2] M. Brando, D. Belitz, F. M. Grosche, and T. R. Kirkpatrick, *Rev. Mod. Phys.* **88**, 025006 (2016).
- [3] J. A. Mydosh, *Adv. Phys.* **66**, 263 (2017).
- [4] J. Faber and G. H. Lander, *Phys. Rev. B* **14**, 1151 (1976).
- [5] P. Giannozzi and P. Erdős, *J. Magn. Magn. Mater.* **67**, 75 (1987).
- [6] P. Santini, S. Carretta, G. Amoretti, R. Caciuffo, N. Magnani, and G. H. Lander, *Rev. Mod. Phys.* **81**, 807 (2009).
- [7] M. Jaime, A. Saul, M. Salamon, V. S. Zapf, N. Harrison, T. Durakiewicz, J. C. Lashley, D. A. Andersson, C. R. Staneck, J. L. Smith, and K. Gofryk, *Nat. Commun.* **8**, 99 (2017).
- [8] K. Andres, D. Davidov, P. Dernier, F. Hsu, W. A. Reed, and G. J. Nieuwenhuys, *Solid State Commun.* **28**, 405 (1978).
- [9] K. A. McEwen, U. Steigenberger, and J. L. Martinez, *Phys. B (Amsterdam)* **186-188**, 670 (1993).
- [10] H. C. Walker, K. A. McEwen, D. F. McMorro, S. B. Wilkins, F. Wastin, E. Colineau, and D. Fort, *Phys. Rev. Lett.* **97**, 137203 (2006).
- [11] B. Becker, S. Ramakrishnan, A. A. Menovsky, G. J. Nieuwenhuys, and J. A. Mydosh, *Phys. Rev. Lett.* **78**, 1347 (1997).
- [12] T. Takeuchi, T. Yamada, Y. Miyako, K. Oda, K. Kindo, B. Becker, S. Ramakrishnan, A. A. Menovsky, G. J. Nieuwenhuys, and J. A. Mydosh, *Phys. Rev. B* **56**, 10778 (1997).
- [13] R. Feyerherm, C. R. Wiebe, B. D. Gaulin, M. F. Collins, B. Becker, R. W. A. Hendrikx, T. J. Gortenmulder, G. J. Nieuwenhuys, and J. A. Mydosh, *Phys. Rev. B* **56**, 13693 (1997).
- [14] R. G. Leisure, S. Kern, F. R. Drymiotis, H. Ledbetter, A. Migliori, and J. A. Mydosh, *Phys. Rev. Lett.* **95**, 075506 (2005).
- [15] Y.-L. Wang and B. R. Cooper, *Phys. Rev.* **172**, 539 (1968).
- [16] Y.-L. Wang and B. R. Cooper, *Phys. Rev.* **185**, 696 (1969).
- [17] E. Hickey, B. Chevalier, P. Gravereau, and J. Etourneau, *J. Magn. Magn. Mater.* **90-91**, 501 (1990).
- [18] F. Galli, R. Feyerherm, K. Prokes, and G. J. Nieuwenhuys, *Phys. B (Amsterdam)* **276-278**, 632 (2000).
- [19] <https://mgml.eu/>.
- [20] Y. Haga, T. Honma, E. Yamamoto, H. Ohkuni, Y. Ōnuki, M. Ito, and N. Kimura, *Jpn. J. Appl. Phys.* **37**, 3604 (1998).
- [21] R. Daou, F. Weickert, M. Nicklas, F. Steglich, A. Haase, and M. Doerr, *Rev. Sci. Instrum.* **81**, 033909 (2010).
- [22] M. Jaime, R. Daou, S. A. Crooker, F. Weickert, A. Uchida, A. E. Feiguin, C. D. Batista, H. A. Dabkowska, and B. D. Gaulin, *Proc. Natl. Acad. Sci. U. S. A.* **109**, 12404 (2012).
- [23] M. Jaime, C. C. Moya, F. Weickert, V. Zapf, F. Balakirev, M. Wartenbe, P. Rosa, J. Betts, G. Rodriguez, S. Crooker, and R. Daou, *Sensors* **17**, 2572 (2017).
- [24] J. A. Detwiler, G. M. Schmiedeshoff, N. Harrison, A. H. Lacerda, J. C. Cooley, and J. L. Smith, *Phys. Rev. B* **61**, 402 (2000).
- [25] B. Becker, A. C. Wallast, J. A. A. J. Perenboom, G. J. Nieuwenhuys, and J. A. Mydosh, *Phys. B (Amsterdam)* **259-261**, 250 (1999).
- [26] A. R. Mackintosh, *Phys. Rev. Lett.* **9**, 90 (1962).
- [27] R. J. Elliott and F. A. Wedgwood, *Proc. Phys. Soc., London* **81**, 846 (1963).
- [28] D. E. Hegland, S. Legvold, and F. H. Spedding, *Phys. Rev.* **131**, 158 (1963).
- [29] S. A. M. Mentink, T. E. Mason, S. Süllow, G. J. Nieuwenhuys, A. A. Menovsky, J. A. Mydosh, and J. A. A. J. Perenboom, *Phys. Rev. B* **53**, R6014 (1996).
- [30] Close and comparative inspection of the AFM transition as seen in susceptibility and resistivity indicates that the value of $T_N(\rho)$ is consistently slightly higher than the value of $T_N(\chi)$. We believe that this reflects the first-order nature of the phase transition, leading to the coexistence of paramagnetic and anti-ferromagnetic phase volume. With the drop in the resistivity in the AFM phase, as a transport technique the resistivity will be more sensitive to the onset of magnetic order, as it will probe the percolative resistance path provided by the low-resistive AFM phase. In contrast, susceptibility and magnetostriction will more closely reflect the phase volume of the AFM phase, leading to the effectively smaller T_N seen with these techniques.
- [31] J. Rossat-Mignod, P. Burlet, J. Villain, H. Bartholin, W. Tcheng-Si, D. Florence, and O. Vogt, *Phys. Rev. B* **16**, 440 (1977).
- [32] E. Brück, H. Nakotte, F. R. de Boer, P. F. de Châtel, H. P. van der Meulen, J. J. M. Franse, A. A. Menovsky, N. H. Kim-Ngan, L. Havela, V. Sechovsky, J. A. A. J. Perenboom, N. C. Tuan, and J. Sebek, *Phys. Rev. B* **49**, 8852 (1994).
- [33] D. Schulze Grachtrup, M. Bleckmann, B. Willenberg, S. Süllow, M. Bartkowiak, Y. Skourski, H. Rakoto, I. Sheikin, and J. A. Mydosh, *Phys. Rev. B* **85**, 054410 (2012).
- [34] D. S. Grachtrup, N. Steinki, S. Süllow, Z. Cakir, G. Zwignagl, Y. Krupko, I. Sheikin, M. Jaime, and J. A. Mydosh, *Phys. Rev. B* **95**, 134422 (2017).
- [35] K. Shrestha, D. Antonio, M. Jaime, N. Harrison, D. S. Mast, D. Safarik, T. Durakiewicz, J.-C. Griveau, and K. Gofryk, *Sci. Rep.* **7**, 6642 (2017).
- [36] R. L. Stillwell, I.-L. Liu, N. Harrison, M. Jaime, J. R. Jeffries, and N. P. Butch, *Phys. Rev. B* **95**, 014414 (2017).
- [37] J. Valenta, F. Honda, M. Vališka, P. Opletal, J. Kaštil, M. Míšek, M. Diviš, L. Sandratskii, J. Prchal, and V. Sechovský, *Phys. Rev. B* **97**, 144423 (2018).
- [38] J. Pospíšil, Y. Haga, Y. Kohama, A. Miyake, S. Kambe, N. Tateiwa, M. Vališka, P. Proschek, J. Prokleška, V. Sechovský,

- M. Tokunaga, K. Kindo, A. Matsuo, and E. Yamamoto, *Phys. Rev. B* **98**, 014430 (2018).
- [39] J. Pospíšil, J. Gouchi, Y. Haga, F. Honda, Y. Uwatoko, N. Tateiwa, S. Kambe, S. Nagasaki, Y. Homma, and E. Yamamoto, *J. Phys. Soc. Jpn.* **86**, 044709 (2017).
- [40] M. Samsel-Czekala, E. Talik, P. deV. Du Plessis, R. Troć, H. Misiorek, and C. Sułkowski, *Phys. Rev. B* **76**, 144426 (2007).
- [41] R. Wawryk, *Philos. Mag.* **86**, 1775 (2006).
- [42] B. Becker, N. G. Patil, S. Ramakrishnan, A. A. Menovsky, G. J. Nieuwenhuys, J. A. Mydosh, M. Kohgi, and K. Iwasa, *Phys. Rev. B* **59**, 7266 (1999).
- [43] M. H. Jung, H. C. Kim, A. Migliori, F. Galli, and J. A. Mydosh, *Phys. Rev. B* **68**, 132102 (2003).